RESEARCH ARTICLE

National Science Review
7: 737–744, 2020
doi: 10.1093/nsr/nwz223
Advance access publication 8 January 2020

MATERIALS SCIENCE

Ultrafast growth of large single crystals of monolayer WS_2 and WSe_2

Zhengwei Zhang[1], Peng Chen[1], Xiangdong Yang[1], Yuan Liu[2], Huifang Ma[1], Jia Li[1], Bei Zhao[1], Jun Luo[3], Xidong Duan[1,*] and Xiangfeng Duan[4]

[1]State Key Laboratory for Chemo/Biosensing and Chemometrics, College of Chemistry and Chemical Engineering, Hunan University, Changsha 410082, China; [2]Department of Applied Physics, School of Physics and Electronics, Hunan University, Changsha 410082, China; [3]Center for Electron Microscopy, Institute for New Energy Materials and Low-Carbon Technologies, School of Materials, Tianjin University of Technology, Tianjin 300384, China and [4]Department of Chemistry and Biochemistry, University of California, Los Angeles, CA 90095, USA

*Corresponding author. E-mail: xidongduan@hnu.edu.cn

Received 27 September 2019; **Revised** 13 December 2019; **Accepted** 23 December 2019

ABSTRACT

Monolayer transition metal dichalcogenides (TMDs) have attracted considerable attention as atomically thin semiconductors for the ultimate transistor scaling. For practical applications in integrated electronics, large monolayer single crystals are essential for ensuring consistent electronic properties and high device yield. The TMDs available today are generally obtained by mechanical exfoliation or chemical vapor deposition (CVD) growth, but are often of mixed layer thickness, limited single crystal domain size or have very slow growth rate. Scalable and rapid growth of large single crystals of monolayer TMDs requires maximization of lateral growth rate while completely suppressing the vertical growth, which represents a fundamental synthetic challenge and has motivated considerable efforts. Herein we report a modified CVD approach with controllable reverse flow for rapid growth of large domain single crystals of monolayer TMDs. With the use of reverse flow to precisely control the chemical vapor supply in the thermal CVD process, we can effectively prevent undesired nucleation before reaching optimum growth temperature and enable rapid nucleation and growth of monolayer TMD single crystals at a high temperature that is difficult to attain with use of a typical thermal CVD process. We show that monolayer single crystals of 450 μm lateral size can be prepared in 10 s, with the highest lateral growth rate up to 45 μm/s. Electronic characterization shows that the resulting monolayer WSe_2 material exhibits excellent electronic properties with carrier mobility up to 90 $cm^2\ V^{-1}\ s^{-1}$, comparable to that of the best exfoliated monolayers. Our study provides a robust pathway for rapid growth of high-quality TMD single crystals.

Keywords: monolayer transition metal dichalcogenides, large single crystal, CVD, ultrafast growth

INTRODUCTION

Two-dimensional (2D) transition metal dichalcogenides (TMDs) have attracted considerable attention for their distinct physical properties, such as atomically thin geometry, extraordinary mechanical flexibility, layer-number dependent electronic and optoelectronic properties, and tunable spin and valley polarization [1–4], and their potential applications in 2D electronics, optoelectronics and spintronics [5–14]. However, the studies to date are largely limited to mechanically exfoliated materials with limited yield and size. Scalable growth of large area monolayer TMDs is indispensable for practical applications, and has motivated considerable efforts in developing synthetic strategies to high-quality large area TMD monolayers or few layers, including solid-source chemical vapor deposition (CVD) [9,15–38], and gas source metal-organic CVD [39,40]. Of note, yielding much larger crystal size and incurring less contamination by other unwanted elements (necessary in organometallic precursors), the materials produced by solid-source CVD are often of much higher electronic quality. Recently, wafer-scale growth of 2D crystals (polycrystalline) has also been demonstrated with the use of a solid-source CVD approach [41,42]. Despite significant advancements, the materials produced to date are often of mixed layer thickness, limited single crystal domain size or have slow growth rate, limiting the ability to ensure growth of exclusive monolayer materials over large lateral dimension.

For practical applications of these 2D materials in electronic and optoelectronic devices, growth of

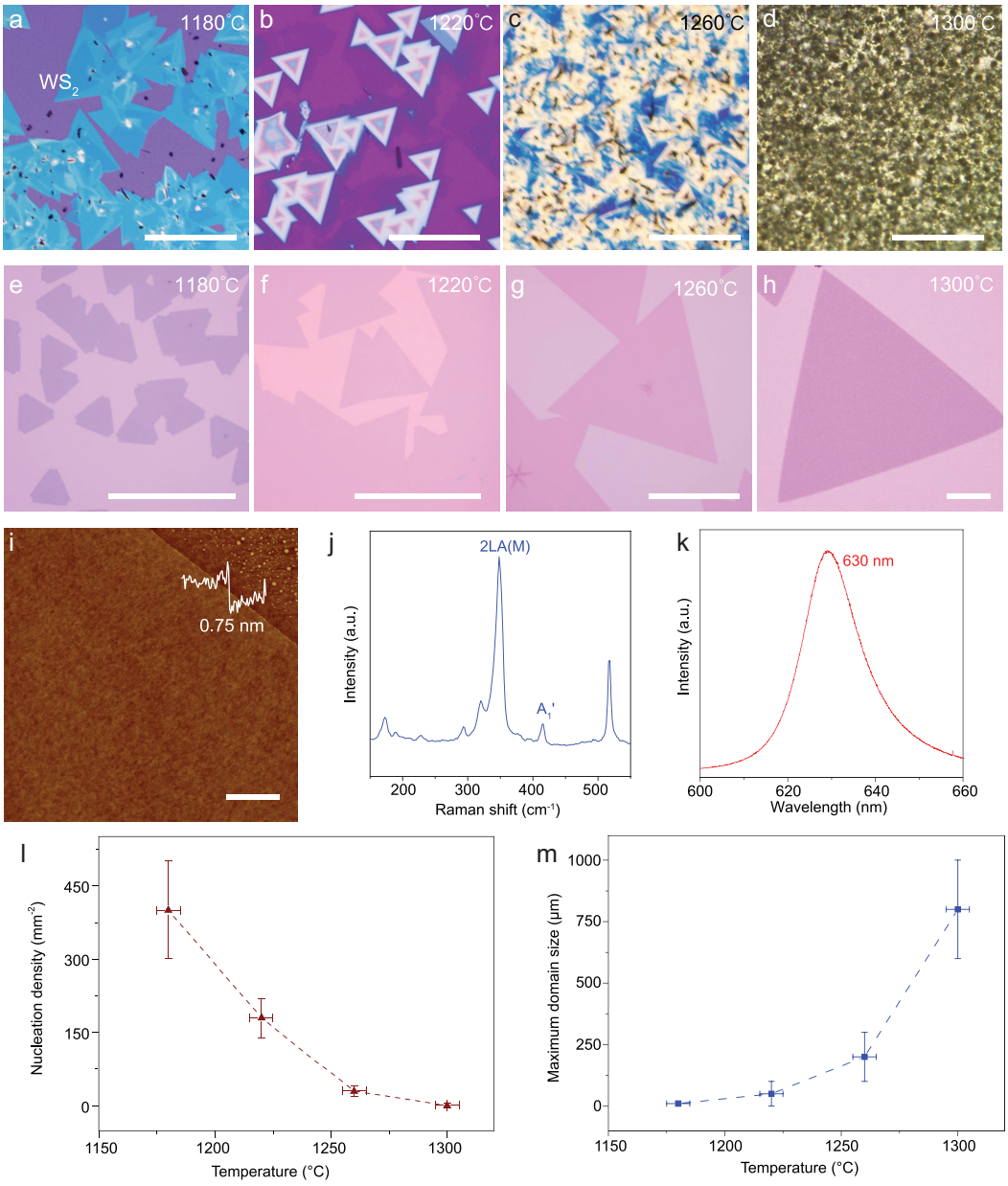

Figure 1. Growth of monolayer WS_2 single crystals. (a–h) Optical microscope (OM) images of WS_2 growth with the use of a conventional CVD process (a–d) and a modified CVD process with reverse flow (e–h) kept at different temperatures for 10 s. (i) AFM image and thickness of the monolayer WS_2 single crystal. (j, k) Raman and photoluminescence spectra of the monolayer WS_2 single crystal. (l, m) The average nucleation density vs. growth temperature (l) and the maximum domain size vs. the growth temperature (m). Scale bars: 100 μm (a–g), 200 μm (h) and 1 μm (i). Note that we focus on the largest domain here for evaluating the growth rate as smaller domains can also occur where new nuclei form during the middle of the growth period.

large single crystal domains with no grain boundaries is essential for ensuring consistent electronic properties and high device yield. To this end, it is essential to reduce nucleation density in the CVD process [43,44]. This is often achieved by keeping the vapor phase source supply sufficiently low to minimize the probability of nucleation of new crystals and prevent multi-layer formation; however, this markedly slows the lateral growth rate (typically ~1 μm/s or less) [20,31,34]. Large domain monolayer single crystals are usually achieved by extending the growth time, and it often takes hours or even longer to achieve millimeter-scale monolayer crystals [31,43]. Maximizing the lateral growth rate while minimizing the vertical growth for efficient production of large domain monolayer single crystals represents a

critical challenge in 2D crystal growth, and is a topic of considerable fundamental and practical significance [45–48]. With use of specifically designed or catalyzed CVD processes, the lateral growth rate of monolayer graphene can be greatly boosted up to 200 μm/s [44].

Rapid growth of monolayer TMD single crystals is more complicated because of difficulties in controlling vapor phase reactants from the vaporization of solid-source materials or organometallics (vs. the simple methane gas for graphene), and has been insufficiently explored to date. In general, rapid growth of large single crystals requires sufficient precursor supply and a sufficient surface migration rate for the precursors, so that once a monolayer nucleus forms, the precursors can rapidly diffuse to and attach onto the growing crystal before new nuclei form. In this case, a higher temperature is usually desired to ensure sufficient source supply and high surface migration rate. However, in a typical thermal CVD process with solid sources, the higher temperature usually leads to rapid increase of source evaporation and unintentional supply of vapor phase reactant before reaching the targeted growth temperature, resulting in ill-controlled nucleation and growth during the temperature ramping stage to produce highly heterogeneous thin films.

Herein, we employ a reverse flow reactor to ensure highly controlled nucleation and growth at high temperature and enable ultrafast growth of millimeter-scale monolayer TMD single crystals. Specifically, we use the reverse gas flow from the substrate to the source during the temperature ramping stage to prevent the unintended supply of the chemical vapor phase reactant during the temperature ramping stage (Supplementary Fig. S1) [49]. This approach can effectively prevent uncontrolled nucleation and growth before reaching optimum growth temperature, making it possible to reach a higher growth temperature to ensure a sufficient vapor phase reactant supply and sufficient surface migration rate for the rapid growth of large single crystals.

RESULTS

Although monolayer TMDs have been successfully produced under precisely controlled conditions with use of a typical thermal CVD process, synthetic conditions are usually highly sensitive [19,21,50]. In this process, the precursor vapor supply is generated by thermal evaporation of solid source and carried downstream to initiate nucleation and growth of 2D crystals on the growth substrate. Here the chemical vapor source is continuously generated and unintentionally supplied to the growth substrate during the temperature ramping stage. Such unintentional supply of the chemical vapor source leads to undesired nucleation and growth before reaching the optimum growth temperature. This makes it particularly difficult to explore the use of a high growth temperature (which is desired for rapid growth of large single crystals), because the higher the designated growth temperature, the greater the unintended chemical vapor supply before reaching the designated growth temperature, which leads to highly heterogeneous thin film deposition with poor control of the thickness and domain size (Fig. 1a–d). For this reason, to minimize excessive vapor supply and undesired material deposition during the temperature ramping stage, growth is typically carried out at a lower temperature (e.g., <1200°C for the source temperature) with a rather low lateral growth rate (~1 μm/s or less). To break this critical limit, we employed reverse flow during the temperature ramping stage to minimize the undesired supply of gas phase reactants to the growth substrate before reaching the optimum growth temperature, thus enabling rapid growth of large size monolayer single crystals (Fig. 1e, f). An atomic force microscope (AFM)

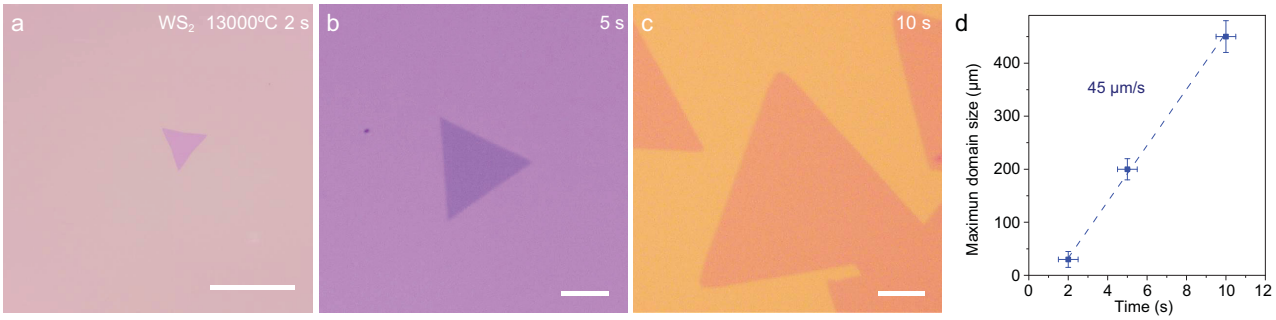

Figure 2. Determination of the maximum growth rate. (a–c) OM images of WS_2 synthesized at $t = 2$ s (a), 5 s (b) and 10 s (c), respectively. (d) Plot and fit of the maximum domain size of WS_2 as a function of growth time. The slope reveals an ultrafast growth rate of ~45 μm s^{-1}. All scale bars are 100 μm.

image of the sample shows that the thickness of the resulting WS_2 single crystal is around 0.75 nm (line scan in Fig. 1i), indicating successful growth of monolayer WS_2. A typical Raman spectrum of the WS_2 sample exhibits two prominent peaks at 350 cm^{-1} and 419 cm^{-1} corresponding to the 2LA(M) and A_1' resonance modes of monolayer WS_2 (Fig. 1b) [51]. The photoluminescence (PL) spectrum of the sample (Fig. 1c) shows a single peak at 630 nm, also consistent with direct bandgap emission of monolayer WS_2.

After minimizing the unintentional supply at the temperature ramping stage, we found that nucleation density decreases rapidly with increasing growth temperature (Fig. 1l), which is essential for achieving large single crystal domains and consistent with previous studies on graphene and TMD growth [43,52]. At the same time, the monolayer domain size increases rapidly with the increased growth temperature (Fig. 1m). The maximum domain size reached 800 μm at 1300°C. Note that the temperature we present is the temperature of the source materials. In our single-temperature-zone setup, the substrate temperature is generally lower than the source temperature (Supplementary Table S2).

We further performed a time-dependent growth experiment to evaluate the domain growth speed. Figure 2a–c illustrates the optical images of WS_2 single crystals at different growth times t ($T = 1300$°C). $t = 0$ s is defined as the moment at which the flow direction is switched on reaching the designated growth temperature. At time t, the growth was quenched by shutting off the chemical supply and rapidly pulling the quartz tube out from the furnace (Supplementary Fig. S2). We found a growth rate of up to 45 μm/s (Fig. 2d), exceeding the highest growth speed previously reported for TMDs (~26 μm/s) (Supplementary Table S3).

This ultrafast growth of large monolayer single TMD crystals could be attributed to both the enhanced source supply and increased surface migration rate at a higher temperature, which was not achievable in previous studies. A higher source temperature can promote evaporation of source materials, and enable a rapid lateral growth rate. In addition, the substrate temperature also increased with the source temperature. A higher substrate temperature can enhance the atom migration, as described by the migration equation: $D \approx D_\infty \exp(-U/k_B T)$, where k_B is the Boltzmann constant and U is the migration barrier energy.

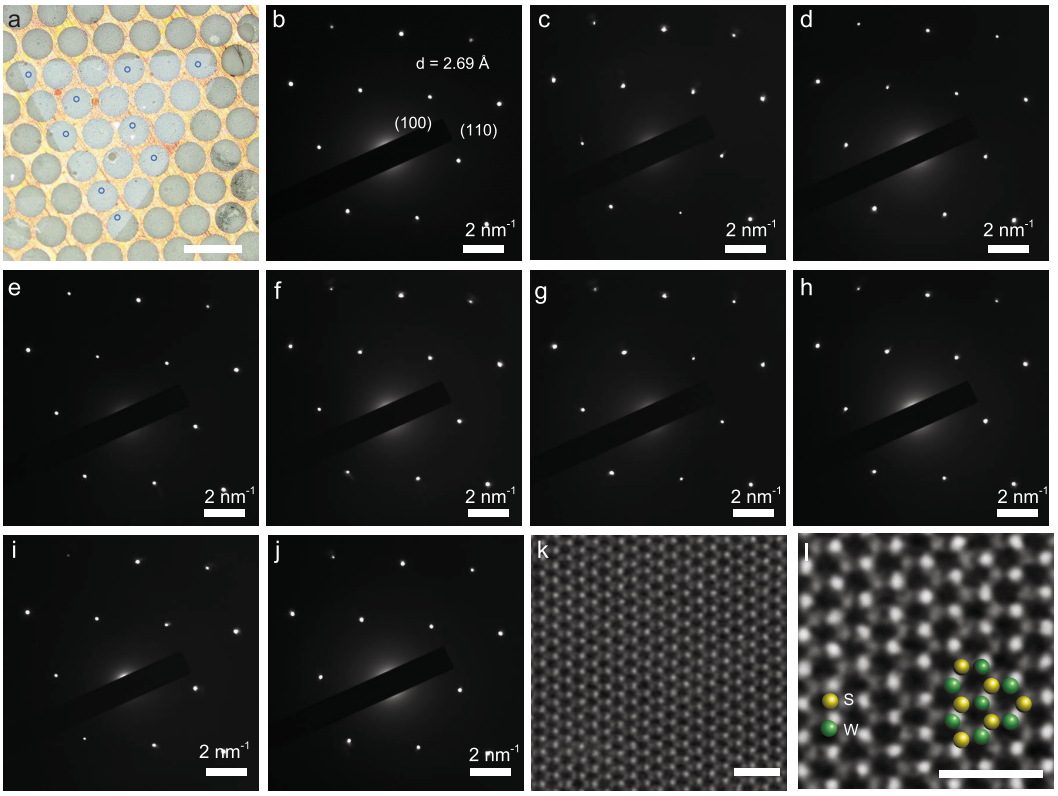

Figure 3. TEM study of monolayer WS_2 single crystals. (a) OM image of a 900-μm WS_2 crystal transferred onto a TEM grid. The scale bar is 200 μm. (b–j) Nine SAED patterns from the areas labeled in (a). (k, l) STEM images of WS_2 crystals. Scale bars are 1 nm.

At higher temperatures, the migration coefficient is larger and adatoms can diffuse over longer distances before attaching to an island. Recent theoretical calculations showed that the migration energies of W and S atoms on the edge site of WS_2 are about 3.81 eV and 1.02 eV, respectively [53]. Thus, the lateral growth of WS_2 is mainly limited by W migration with a migration barrier of 3.81 eV. According to the migration equation, when the substrate temperature increased from 753°C to 875°C (the source temperature increased from 1150°C to 1300°C), the migration coefficient at 875°C will be ~82 times larger than that at 753°C. This significantly accelerated atom migration at higher temperature can enable rapid lateral growth of monolayer single crystals.

To evaluate the quality of the large single crystals obtained with the ultrafast growth method, we further investigated the microstructure of the resulting monolayer WS_2 single crystals using selected area electron diffraction (SAED) and high-angle annular dark-field scanning transmission electron microscope (STEM). Figure 3a shows an OM image of a single monolayer WS_2 domain (~900 μm) transferred onto a transmission electron microscope (TEM) grid. The SAED patterns acquired from nine representative areas (as labeled in Fig. 3a) show a single set of hexagonally arranged diffraction spots with identical orientations (Fig. 3b–j), suggesting a single-crystalline lattice structure throughout the entire WS_2 domain. The atomically resolved STEM image (Fig. 3k, l), with the brighter/dimmer areas corresponding to W/S atoms, shows that the WS_2 domain exhibits an almost perfect lattice structure with no obvious vacancies and topological defects, confirming the high crystalline quality of the WS_2 samples.

To assess the generality of the reverse flow approach for growth of monolayer single crystals of

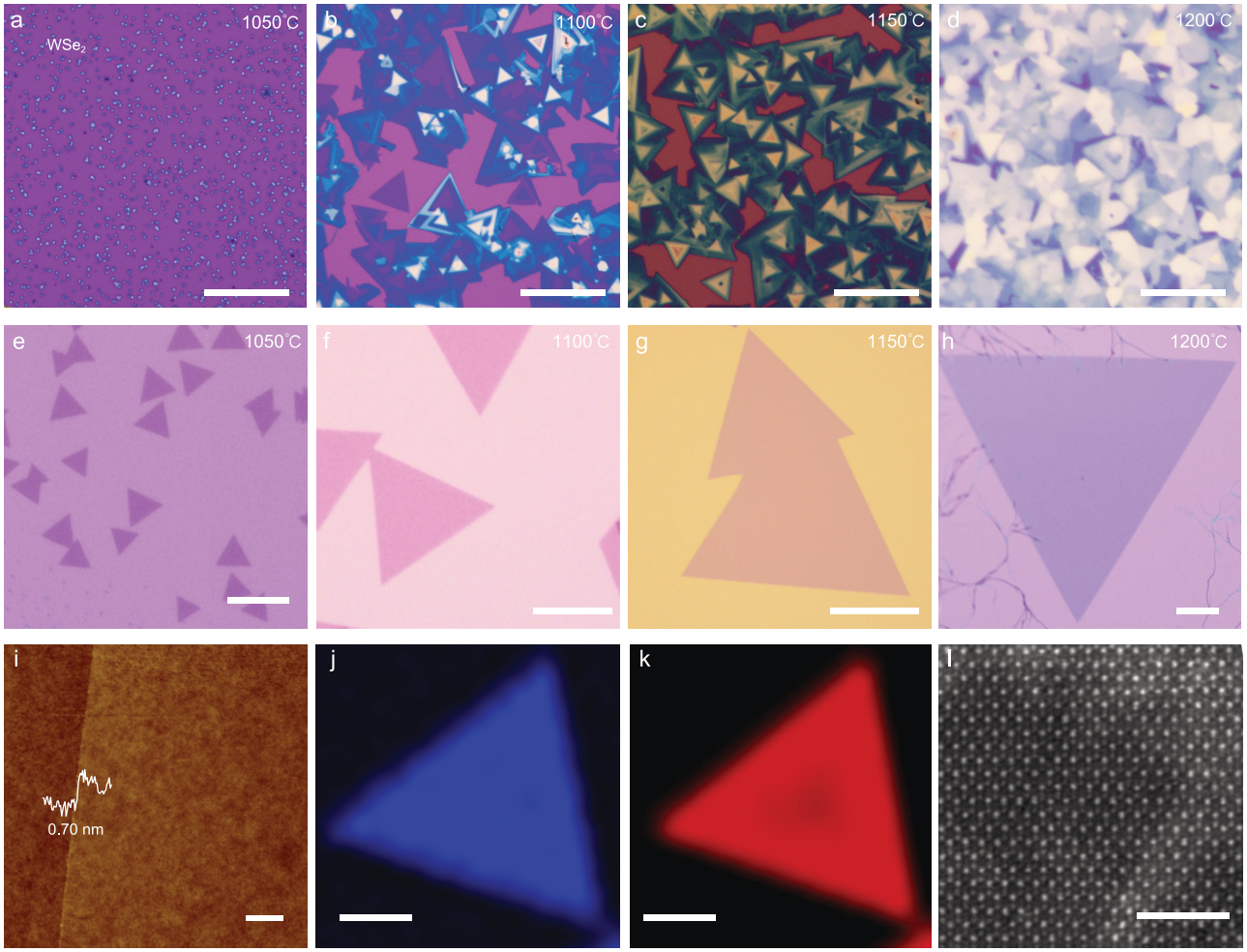

Figure 4. Ultrafast growth of monolayer WSe_2 single crystals. (a–h) OM images of WSe_2 grown with a conventional CVD process (a–d) and a modified CVD process with reverse flow (e–h) kept at different temperatures for 10 s. (i) AFM image and thickness of the WSe_2 single crystal. (j, k) Raman (j) and PL (k) spectroscopy maps of the peaks at 250 cm^{-1} and 760 nm of the monolayer WSe_2 domain. (l) STEM image of a monolayer WSe_2 crystal. Scale bars: 10 μm in (e), 100 μm in (a–d, f–h, j, k), 2 nm in (i).

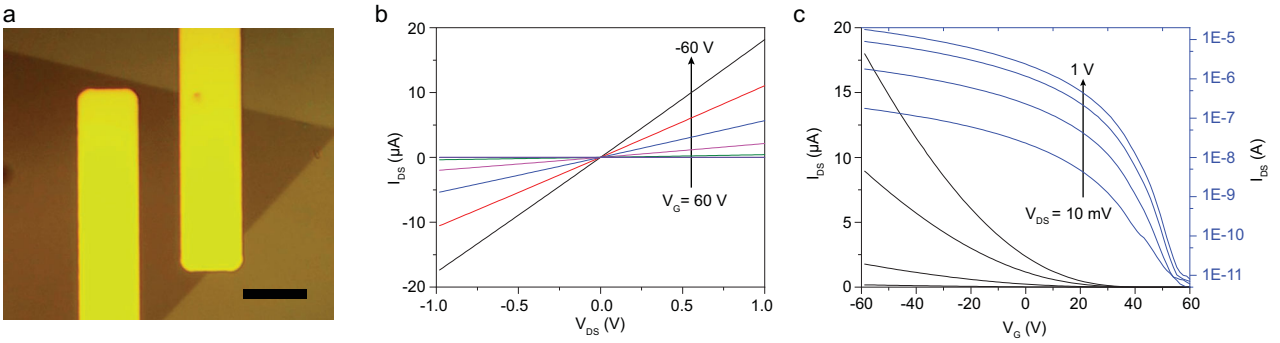

Figure 5. Electronic properties of the monolayer WSe_2 prepared by the ultrafast growth. (a) OM image of a monolayer WSe_2 transistor with two transferred Pt electrodes on Si/SiO_2 substrate; the scale bar is 10 μm. (b) I_{DS}—V_{DS} output characteristics of a typical WSe_2 transistor. (c) I_{DS}—V_G transfer characteristics at V_{DS} = 10 mV, 100 mV, 500 mV and 1 V. The black and blue curves are the linear plot and semi-log plot, respectively.

other TMDs, we also applied this approach to grow monolayer WSe_2 single crystals. Similarly, a conventional CVD process produces highly heterogeneous thin films at a high temperature (Fig. 4a–d), whereas the modified CVD method with reverse flow produces highly uniform monolayer single crystals (Fig. 4e–h), with increasingly larger WSe_2 domains obtained at higher temperature. The size of the WSe_2 crystals can reach 800 μm (Fig. 4f), with the highest growth rate being ~20 μm/s (Supplementary Fig. S3). An AFM image shows that the thickness of the resulting WSe_2 single crystal is around 0.70 nm (Fig. 4i). Raman spectroscopic studies show a single prominent peak at 250 cm^{-1}, corresponding to the A_1' resonance mode of monolayer WSe_2 (Supplementary Fig. S4a), and the PL spectrum shows a single peak at 760 nm (Supplementary Fig. S4b), consistent with the direct bandgap emission of monolayer WSe_2. The corresponding Raman and PL maps of the monolayer WSe_2 single crystal domain show a highly uniform contrast (Fig. 4j, k), indicating the high crystalline homogeneity of the monolayer WSe_2 domain. Furthermore, the STEM image confirms an almost perfect lattice structure (Fig. 4l).

To investigate the electrical properties of the resulting monolayer crystals, back-gate field-effect transistors (FETs) were fabricated on SiO_2/Si substrates with transferred Pt contact electrodes (Fig. 5a) [54]. The I_{DS}-V_{DS} characteristics of a typical monolayer WSe_2 FET show linear and symmetric curves (Fig. 5b), suggesting Ohmic-like contacts. Transfer curves at different V_G show that the I_{DS} value decreases monotonically with increasing V_G (Fig. 5c), indicating p-type behavior. The measured on/off ratio reaches 2×10^6 at a source-drain bias of 1 V. The carrier mobility can be calculated from the linear regime of the transfer characteristics. Notably, the highest mobility of 90 $cm^2 V^{-1} s^{-1}$ was achieved in monolayer WSe_2 FETs, which is comparable to the best values reported previously for exfoliated monolayer materials and confirms the high crystalline quality of our WSe_2 crystals [55].

CONCLUSION

In conclusion, we have developed a modified CVD process using reverse flow during the temperature ramping stage to prevent the unintended supply of chemical vapor source and uncontrolled nucleation and growth, thus greatly enhancing the controllability of the chemical vapor supply and enabling controlled nucleation and rapid growth of millimeter-size-scale monolayer single crystals. Optical and STEM studies reveal the excellent crystalline quality of the resulting 2D crystals. Electrical transport studies further demonstrate that the 2D crystals exhibit excellent electronic characteristics. Thus, our study defines a robust approach to high-quality large-sized 2D single crystals, which is essential for future application of 2D materials in integrated electronics and optoelectronics.

SUPPLEMENTARY DATA

Supplementary data are available at *NSR* online.

FUNDING

This work was supported by the National Natural Science Foundation of China (51872086 and 51991343), the Fundamental Research Funds of the Central Universities (531107051078), the Double First-Class Initiative of Hunan University (531109100004) and the Hunan Key Laboratory of Two-Dimensional Materials (2018TP1010).

Conflict of interest statement. None declared.

REFERENCES

1. Geim AK and Grigorieva IV. Van der Waals heterostructures. *Nature* 2013; **499**: 419–25.
2. Mak KF, Lee C and Hone J *et al.* Atomically thin MoS_2: a new direct-gap semiconductor. *Phys Rev Lett* 2010; **105**: 136805.
3. Ross JS, Klement P and Jones AM *et al.* Electrically tunable excitonic light-emitting diodes based on monolayer WSe_2 p-n junctions. *Nat Nanotechnol* 2014; **9**: 268–72.
4. Rivera P, Seyler KL and Yu H *et al.* Valley-polarized exciton dynamics in a 2D semiconductor heterostructure. *Science* 2016; **351**: 688–91.
5. Splendiani A, Sun L and Zhang Y *et al.* Emerging photoluminescence in monolayer MoS_2. *Nano Lett* 2010; **10**: 1271–5.
6. Wang QH, Kalantar-Zadeh K and Kis A *et al.* Electronics and optoelectronics of two-dimensional transition metal dichalcogenides. *Nat Nanotechnol* 2012; **7**: 699–712.
7. Yin Z, Li H and Li H *et al.* Single-layer MoS_2 phototransistors. *ACS Nano* 2012; **6**: 74–80.
8. Zhao M, Ye Y and Han Y *et al.* Large-scale chemical assembly of atomically thin transistors and circuits. *Nat Nanotechnol* 2016; **11**: 954–9.
9. Van Der Zande AM, Huang PY and Chenet DA *et al.* Grains and grain boundaries in highly crystalline monolayer molybdenum disulphide. *Nat Mater* 2013; **12**: 554–61.
10. Huang C, Wu S and Sanchez AM *et al.* Lateral heterojunctions within monolayer $MoSe_2$-WSe_2 semiconductors. *Nat Mater* 2014; **13**: 1096–101.
11. Zhou F, Zhou Z and Chen J *et al.* Optoelectronic resistive random access memory for neuromorphic vision sensors. *Nat Nanotechnol* 2019; **14**: 776–82.
12. Xiang D, Liu T and Xu J *et al.* Two-dimensional multibit optoelectronic memory with broadband spectrum distinction. *Nat Commun* 2018; **9**: 2966.
13. Chen X, Shehzad K and Gao L *et al.* Graphene hybrid structures for integrated and flexible optoelectronics. *Adv Mater* 2019; doi: 10.1002/adma.201902039.
14. Tian H, Chin ML and Najmaei S *et al.* Optoelectronic devices based on two-dimensional transition metal dichalcogenides. *Nano Res* 2016; **9**: 1543–60.
15. Najmaei S, Liu Z and Zhou W *et al.* Vapour phase growth and grain boundary structure of molybdenum disulphide atomic layers. *Nat Mater* 2013; **12**: 754–9.
16. Zhou J, Lin J and Huang X *et al.* A library of atomically thin metal chalcogenides. *Nature* 2018; **556**: 355–9.
17. Yang P, Zou X and Zhang Z *et al.* Batch production of 6-inch uniform monolayer molybdenum disulfide catalyzed by sodium in glass. *Nat Commun* 2018; **9**: 979.
18. Wang X, Feng H and Wu Y *et al.* Controlled synthesis of highly crystalline MoS_2 flakes by chemical vapor deposition. *J Am Chem Soc* 2013; **135**: 5304–7.
19. Duan X, Wang C and Shaw JC *et al.* Lateral epitaxial growth of two-dimensional layered semiconductor heterojunctions. *Nat Nanotechnol* 2014; **9**: 1024–30.
20. Chen W, Zhao J and Zhang J *et al.* Oxygen-assisted chemical vapor deposition growth of large single-crystal and high-quality monolayer MoS_2. *J Am Chem Soc* 2015; **137**: 15632–5.
21. Duan X, Wang C and Fan Z *et al.* Synthesis of $WS_{2x}Se_{2-2x}$ alloy nanosheets with composition-tunable electronic properties. *Nano Lett* 2016; **16**: 264–9.
22. Li M-Y, Shi Y and Cheng C-C *et al.* Epitaxial growth of a monolayer WSe2-MoS2 lateral p-n junction with an atomically sharp interface. *Science* 2015; **349**: 524–8.
23. Chen J, Zhao X and Tan SJ *et al.* Chemical vapor deposition of large-size monolayer $MoSe_2$ crystals on molten glass. *J Am Chem Soc* 2017; **139**: 1073–6.
24. Gong Y, Lin J and Wang X *et al.* Vertical and in-plane heterostructures from WS_2/MoS_2 monolayers. *Nat Mater* 2014; **13**: 1135–42.
25. Kang K, Xie S and Huang L *et al.* High-mobility three-atom-thick semiconducting films with wafer-scale homogeneity. *Nature* 2015; **520**: 656–60.
26. Mahjouri-Samani M, Lin M-W and Wang K *et al.* Patterned arrays of lateral heterojunctions within monolayer two-dimensional semiconductors. *Nat Commun* 2015; **6**: 7749.
27. Chen J, Zhou W and Tang W *et al.* Lateral epitaxy of atomically sharp WSe_2/WS_2 heterojunctions on silicon dioxide substrates. *Chem Mater* 2016; **28**: 7194–7.
28. Liu K-K, Zhang W and Lee Y-H *et al.* Growth of large-area and highly crystalline MoS_2 thin layers on insulating substrates. *Nano Lett* 2012; **12**: 1538–44.
29. Lee YH, Zhang XQ and Zhang W *et al.* Synthesis of large-area MoS_2 atomic layers with chemical vapor deposition. *Adv Mater* 2012; **24**: 2320–5.
30. Lee Y-H, Yu L and Wang H *et al.* Synthesis and transfer of single-layer transition metal disulfides on diverse surfaces. *Nano Lett* 2013; **13**: 1852–7.
31. Zhang Y, Zhang Y and Ji Q *et al.* Controlled growth of high-quality monolayer WS_2 layers on sapphire and imaging its grain boundary. *ACS Nano* 2013; **7**: 8963–71.
32. Wang X, Gong Y and Shi G *et al.* Chemical vapor deposition growth of crystalline monolayer $MoSe_2$. *ACS Nano* 2014; **8**: 5125–31.
33. Mann J, Ma Q and Odenthal PM *et al.* 2-Dimensional transition metal dichalcogenides with tunable direct band gaps: $MoS_{2(1-x)}Se_{2x}$ monolayers. *Adv Mater* 2014; **26**: 1399–404.
34. Lu X, Utama MIB and Lin J *et al.* Large-area synthesis of monolayer and few-layer $MoSe_2$ films on SiO_2 substrates. *Nano Lett* 2014; **14**: 2419–25.
35. Kong D, Wang H and Cha JJ *et al.* Synthesis of MoS_2 and $MoSe_2$ films with vertically aligned layers. *Nano Lett* 2013; **13**: 1341–7.
36. Tarasov A, Campbell PM and Tsai MY *et al.* Highly uniform trilayer molybdenum disulfide for wafer-scale device fabrication. *Adv Funct Mater* 2014; **24**: 6389–400.
37. Chen Y, Gan L and Li H *et al.* Achieving uniform monolayer transition metal dichalcogenides film on silicon wafer via silanization treatment: a typical study on WS_2. *Adv Mater* 2017; **29**: 1603550.
38. Chen P, Zhang Z and Duan X *et al.* Chemical synthesis of two-dimensional atomic crystals, heterostructures and superlattices. *Chem Soc Rev* 2018; **47**: 3129–51.
39. Dumcenco D, Ovchinnikov D and Marinov K *et al.* Large-area epitaxial monolayer MoS_2. *ACS Nano* 2015; **9**: 4611–20.
40. Xie S, Tu L and Han Y *et al.* Coherent, atomically thin transition-metal dichalcogenide superlattices with engineered strain. *Science* 2018; **359**: 1131–6.
41. Yu Y, Li C and Liu Y *et al.* Controlled scalable synthesis of uniform, high-quality monolayer and few-layer MoS_2 films. *Sci Rep* 2013; **3**: 1866.
42. Yu H, Liao M and Zhao W *et al.* Wafer-scale growth and transfer of highly-oriented monolayer MoS_2 continuous films. *ACS Nano* 2017; **11**: 12001–7.
43. Zhou H, Yu WJ and Liu L *et al.* Chemical vapour deposition growth of large single crystals of monolayer and bilayer graphene. *Nat Commun* 2013; **4**: 2096.
44. Liu C, Xu X and Qiu L *et al.* Kinetic modulation of graphene growth by fluorine through spatially confined decomposition of metal fluorides. *Nat Chem* 2019; **11**: 730–6.
45. Zhang Z, Xu X and Qiu L *et al.* The way towards ultrafast growth of single-crystal graphene on copper. *Adv Sci* 2017; **4**: 1700087.
46. Yan Z, Peng Z and Tour JM. Chemical vapor deposition of graphene single crystals. *Acc Chem Res* 2014; **47**: 1327–37.
47. Tang S, Wang H and Wang HS *et al.* Silane-catalysed fast growth of large single-crystalline graphene on hexagonal boron nitride. *Nat Commun* 2015; **6**: 6499.

48. Hao Y, Bharathi M and Wang L *et al*. The role of surface oxygen in the growth of large single-crystal graphene on copper. *Science* 2013; **342**: 720–3.
49. Zhang Z, Chen P and Duan X *et al*. Robust epitaxial growth of two-dimensional heterostructures, multiheterostructures, and superlattices. *Science* 2017; **357**: 788–92.
50. Yang T, Zheng B and Wang Z *et al*. Van der Waals epitaxial growth and optoelectronics of large-scale WSe_2/SnS_2 vertical bilayer p-n junctions. *Nat Commun* 2017; **8**: 1906.
51. Berkdemir A, Gutiérrez HR and Botello-Méndez AR *et al*. Identification of individual and few layers of WS_2 using Raman spectroscopy. *Sci Rep* 2013; **3**: 1755.
52. Zhou H, Wang C and Shaw JC *et al*. Large area growth and electrical properties of p-type WSe_2 atomic layers. *Nano Lett* 2015; **15**: 709–13.
53. Wu L, Yang W and Wang G. Mechanism of substrate-induced anisotropic growth of monolayer WS_2 by kinetic Monte Carlo simulations. *npj 2D Mater Appl* 2019; **3**: 6.
54. Liu Y, Guo J and Zhu E *et al*. Approaching the Schottky-Mott limit in van der Waals metal-semiconductor junctions. *Nature* 2018; **557**: 696–700.
55. Movva HCP, Rai A and Kang S *et al*. High-mobility holes in dual-gated WSe_2 field-effect transistors. *ACS Nano* 2015; **9**: 10402–10.